Adsorption heights and bonding strength of organic molecules on a Pb-Ag surface alloy

Benjamin Stadtmüller,[1,2,*] Norman Haag,[1] Johannes Seidel,[1] Gerben van Straaten,[3,4] Markus Franke,[3,4] Christian Kumpf,[3,4] Mirko Cinchetti,[5] and Martin Aeschlimann[1]

[1]*Department of Physics and Research Center OPTIMAS, University of Kaiserslautern, Erwin-Schroedinger-Strasse 46, 67663 Kaiserslautern, Germany*

[2]*Graduate School of Excellence Materials Science in Mainz, Erwin Schroedinger Straße 46, 67663 Kaiserslautern, Germany*

[3]*Peter Grünberg Institut (PGI-3), Forschungszentrum Jülich, 52425 Jülich, Germany*

[4]*Jülich-Aachen Research Alliance (JARA) - Fundamentals of Future Information Technology, 52425 Jülich, Germany*

[5]*Experimentelle Physik VI, Technische Universität Dortmund, 44221 Dortmund, Germany*

(Received 3 August 2016; revised manuscript received 26 October 2016; published 27 December 2016)

The understanding of the fundamental geometric and electronic properties of metal-organic hybrid interfaces is a key issue on the way to improving the performance of organic electronic and spintronic devices. Here, we studied the adsorption heights of copper-II-phthalocyanine (CuPc) and 3,4,9,10-perylene-tetracarboxylic-dianhydride (PTCDA) on a Pb_1Ag_2 surface alloy on Ag(111) using the normal-incidence x-ray standing waves technique. We find a significantly larger adsorption height of both molecules on the Pb-Ag surface alloy compared to the bare Ag(111) surface which is caused by the larger size of Pb. This increased adsorption height suppresses the partial chemical interaction of both molecules with Ag surface atoms. Instead, CuPc and PTCDA molecules bond only to the Pb atoms with different interaction strength ranging from a van der Waals–like interaction for CuPc to a weak chemical interaction with additional local bonds for PTCDA. The different adsorption heights for CuPc and PTCDA on Pb_1Ag_2 are the result of local site-specific molecule-surface bonds mediated by functional molecular groups and the different charge donating and accepting character of CuPc and PTCDA.

DOI: 10.1103/PhysRevB.94.235436

I. INTRODUCTION

One of the great milestones on the way to establishing organic semiconductors as active materials in electronic and spintronic devices is to control the functionality of metal-organic hybrid interfaces according to the device relevant properties. On the way, it was realized that the key to tailoring the geometric and electronic properties of these interfaces is to tune the strength of the molecule-substrate and the intermolecular interactions [1–7]. These interactions are most commonly modified by chemical functionalizing of the organic adsorbates [8–11], by alkali-metal doping of organic monolayer films [12–16], or by the formation of heteromolecular monolayer films containing two different types of molecules [17–22]. All these strategies provided clear pathways to an improved control over the energy level alignment or the lateral order of the molecular monolayer films by changing an external control parameter.

While up to now almost all approaches to design metal-organic interfaces focused on acting on the molecular film itself, it was recently proposed to functionalize metal-organic hybrid interfaces by surface modification, i.e., by controlled substitution of surface atoms of the first metallic layer [23–25]. This attempt is highly interesting for various reasons. On the one hand, metallic substitute atoms in the first metal layer can be used to selectively influence either local molecule-substrate bonds or to provide additional charge for electron doping of the molecular films [23]. On the other hand, the implantation of heavy-metal atoms can be used to create a novel surface band structure with spiral spin texture [24,26]. In the case of a strong hybridization of these metal atoms with molecular orbitals, this could lead to the formation of spin-polarized metal-organic hybrid states [27–29]. The latter are of particular interest in the field of molecular spintronics [30].

Recently, we followed this approach and investigated the adsorption properties of the two prototypical molecules copper-II-phthalocyanine (CuPc) and 3,4,9,10-perylene-tetracarboxylic-dianhydride (PTCDA) adsorbed on a Pb-Ag surface alloy on Ag(111) [25]. In this modified Ag(111) surface, each third silver atoms is replaced by a Pb atom in order to form a long-range-ordered surface alloy. The larger size of the Pb atoms compared to Ag leads to a vertical buckling of the Pb-Ag surface and the hybridization between Ag and Pb atoms results in the formation of two novel hybrid surface states with a spiral spin texture due to the Rashba-Bychkov effect [31,32]. In our previous work, we used the implanted Pb surface atoms as tracer atoms to reveal modifications of the first metallic layer caused by different bonding mechanisms across the metal-organic hybrid interface. We found that for pure van der Waals interactions and for weak delocalized π bonds between the molecule and the surface alloy, the geometric and electronic properties of the first metal layer stay unaffected by the molecular adsorption. In contrast, the formation of local σ-like bonds between the adsorbate and the surface, as in the case for PTCDA on the surface alloy, leads to a vertical relaxation of the Pb atoms and clear modification of the surface band structure.

In this work, we will focus on the molecular side of the interface and reveal how surface alloying alters the vertical adsorption geometry of CuPc and PTCDA on the modified Ag(111) surface. Using the normal-incidence x-ray standing waves (NIXSW) technique, we are able to determine the vertical adsorption position of each chemically different species of CuPc and PTCDA on the surface alloy with very high accuracy (<0.04 Å). Our results show that

*bstadtmueller@physik.uni-kl.de

the molecular bodies of CuPc and PTCDA are found at significantly larger adsorption heights on the surface alloy compared to their adsorption on the bare Ag(111) surface. This is mainly the result of the larger atomic size of the Pb surface atoms that pushes the molecules away from the surface. For CuPc, this reduces any molecule-substrate interaction to a pure physisorption despite its weak chemical interaction with the bare Ag(111) surface [33]. For PTCDA, we find an adsorption-site-specific interaction leading to two different vertical adsorption heights. While PTCDA forms local σ-like bonds between its functional oxygen end groups and the Pb surface atoms for both adsorption sites, the delocalized π bond between the molecular backbone and the Pb-Ag surface alloy depends strongly on the adsorption site. For one adsorption site, we find an at least partial chemical interaction between the π-conjugated part of PTCDA and the Pb surface atoms. For the other PTCDA species, we observe a weak delocalized π-bonding comparable to CuPc on the surface alloy.

The different adsorption behavior of CuPc and PTCDA on the Pb_1Ag_2 surface alloy will be discussed in terms of the different charge donating and charge accepting properties and the additional anhydride oxygen end groups for PTCDA.

II. EXPERIMENTAL DETAILS

A. Sample preparation

All experiments and the sample preparations were performed under ultrahigh-vacuum conditions with base pressure better than 5×10^{-10} mbar. The surface of the (111)-oriented silver crystal was cleaned by repeated cycles of argon ion bombardment and subsequent annealing at a temperature of $T_{\text{sample}} = 730$ K. The cleanliness of the Ag(111) surface was verified either by measuring the surface state at the $\bar{\Gamma}$ point of the surface Brillouin zone or by searching for contaminations in core level spectroscopy. The organic monolayer films on the Pb-Ag surface alloy were prepared in two subsequent steps. First one-third of a monolayer of Pb was deposited onto the clean Ag(111) crystal at elevated sample temperature ($T_{\text{sample}} = 450$ K), followed by sample annealing at $T_{\text{sample}} = 450$ K. This procedure resulted in the formation of a homogeneous well-ordered Pb_1Ag_2 surface alloy in the first layer of the Ag(111) surface. The success of the sample preparation was confirmed by low-energy electron diffraction (LEED) and by photoelectron spectroscopy (PES). Afterwards, CuPc or PTCDA was deposited on the well-ordered Pb_1Ag_2 surface alloy at room temperature. The molecular coverage was controlled by the evaporation time and quantified afterwards by the integrated intensity of characteristic photoemission signals that were normalized to the values of the reference systems PTCDA and CuPc on Ag(111).

B. Normal-incidence x-ray standing waves

The normal-incidence x-ray standing waves (NIXSW) experiments were carried out at the hard x-ray photoemission (HAXPES) and x-ray standing wave (XSW) end station of beamline I09 of the Diamond Light Source (Didcot, UK). This end station is equipped with a hemispherical electron analyzer (Scienta R4000 EW) which is mounted perpendicular to the incoming photon beam. The angular acceptance of the electron analyzer is $\pm 30^\circ$. Due to the experimental geometry (almost normal incidence of photon beam with respect to the surface, $\approx 90^\circ$ emission angle for photoelectrons), half of the angular acceptance cone of the analyzer is shielded by the sample. This effectively reduces the angular acceptance to 30°.

The NIXSW method allows us to determine the vertical adsorption position of all chemically different atomic species within an adsorbate system above a single-crystal substrate with very high precision (<0.04 Å). In the following, we briefly summarize the fundamental aspects of this method. A more detailed introduction can be found elsewhere [34–36]. For a photon energy which fulfills the Bragg condition $\vec{H} = \vec{k}_H - \vec{k}_0$ for a Bragg reflection $\vec{H} = (hkl)$, an x-ray standing wave field is formed by the coherent superposition of the incoming $\vec{E}_0$ and the Bragg-reflected wave $\vec{E}_H$. Scanning the photon energy through the Bragg condition results in a shift of the phase ν of the relative complex amplitude of the incoming and Bragg reflected wave by π. As a consequence, the standing wave field shifts by half a lattice spacing d_{hkl} in the direction perpendicular to the Bragg planes. This changes the photon density at any specific position z above the surface as a function of the photon energy. If an atom is located at this position z, the modification of its x-ray absorption can be monitored by recording the photoemission yield $I(E)$ of any of its core levels. The resulting experimental yield curve $I(E)$ can be modeled by [35,36]

$$I(E) = 1 + R(E) + 2\sqrt{R(E)} + F^H \cos[\nu(E) - 2\pi P^H], \tag{1}$$

where $R(E)$ is the x-ray reflectivity of the Bragg reflection with its complex amplitude $\sqrt{R(E)}$ and phase $\nu(E)$. The actual fit parameters are the coherent position P^H and the coherent fraction F^H. P^H can be interpreted as the average vertical position D^H of an atomic species above the nearest lattice plane of the corresponding Bragg reflection H, which again is related to the true adsorption height z. F^H can usually be understood as a vertical ordering parameter with values between 0 and 1. $F^H = 0$ indicates complete vertical disorder of the emitting atomic species while for $F^H = 1$ all emitters are located at the same adsorption height corresponding to P^H.

During all experiments, we carefully checked for radiation damage. Prior to each NIXSW experiment on a new sample system, we recorded several very short ($\Delta t < 6$ min) NIXSW scans of C 1s (for PTCDA) and N 1s (for CuPc) on the same spot on the sample. A reduction of F^H after a certain exposure time with hard x-ray radiation is a strong indication of radiation damage of the sample. We detected no radiation damage within the first 25 min of x-ray exposure and limited our acquisition time accordingly.

III. RESULTS

After a short discussion of the lateral arrangement of the molecules on the surfaces based on a LEED study, we will present our experimental results of the NIXSW experiments for 1.0 ML CuPc and 0.8 ML PTCDA on the Pb_1Ag_2 surface alloy. In order to determine the vertical positions of all chemically different species, we recorded core data for C 1s, N 1s, O 1s, Cu 2p, and Pb 4f. Using sophisticated fitting

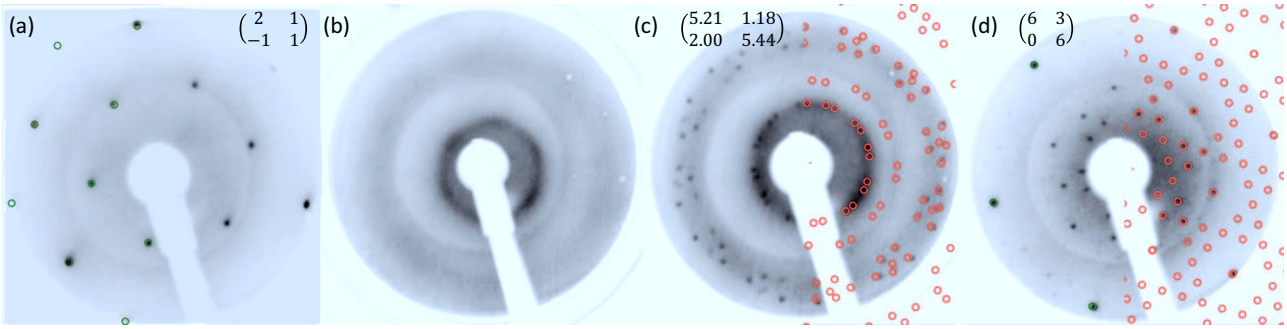

FIG. 1. LEED images of (a) the clean Pb_1Ag_2 surface alloy, (b) a submonolayer film of CuPc/Pb_1Ag_2, (c) a monolayer of CuPc/Pb_1Ag_2, and (d) a monolayer film of PTCDA/Pb_1Ag_2 recorded at (a) $E_{kin} = 92$ eV, (b) 16.5 eV, (c) 22.5 eV, and (d) 35 eV. For panels (a), (c), and (d), calculated diffraction spots are shown as green and red circles, respectively; the corresponding superstructure matrix is also given. For the monolayer PTCDA/Pb_1Ag_2 in panel (d), the calculated positions of the diffraction pattern of the bare Pb_1Ag_2 surface alloy are additionally shown as green circles. For all LEED images, systematic geometric distortions of the LEED data were corrected by means of the software LEEDCAL [37].

models for the C 1*s* and O 1*s* spectra, we were able to disentangle different contributions of chemically different atomic species of PTCDA as well as of structurally inequivalent PTCDA molecules. These models will be employed in the NIXSW analysis to obtain partial-yield curves for all chemically different species. In addition, we can use the results of our core level analysis to gain insight into the chemical environment of the molecules in the molecular films and deduce information about their interaction strength with the substrate.

A. Structure formation

We will start our discussion of the experimental results with an overview of the lateral structure formation of CuPc and PTCDA on the Pb_1Ag_2 surface alloy using LEED. The LEED image of the clean surface alloy in Fig. 1(a) shows the typical diffraction pattern of the $(\sqrt{3} \times \sqrt{3})R30$ superstructure [31]. The calculated positions of the diffraction spots of this superstructure are shown as green circles in the left half of Fig. 1(a). All systematic distortions of the LEED data due to the flat screen of the microchannel plate (MCP) LEED optics were corrected by means of the software LEEDCAL [37].

For CuPc coverages below one monolayer, no additional diffraction spots are visible indicating the lack of a long-range-ordered CuPc structure. Instead, a new ringlike diffraction feature appears around the specular reflection [see Fig. 1(b)] which points to the formation of a 2D lattice gas with an average intermolecular distance reflected by the diameter of the ringlike diffraction feature. Only when the CuPc coverage is increased to one closed layer, the diffraction ring disappears and is replaced the sharp diffraction spots leading to the LEED pattern shown in Fig. 1(c). A similar structural phase diagram has already been reported for various phthalocyanine molecules on the Ag(111) and Au(111) surface and represents the intrinsic growth mode of CuPc on noble-metal surfaces [7,33,38]. Thereby, the structural phase transition from a 2D gaslike phase to a well-ordered monolayer structure is caused by a sterically hindered molecular diffusion on the surface.

More insight into the structural parameters of the CuPc monolayer structure can be obtained by modeling the corresponding diffraction pattern for different superstructure lattices. The best agreement between the experimental and calculated diffraction pattern could be obtained for the superstructure matrix $\begin{pmatrix} 5.32 & 1.18 \\ 2.00 & 5.44 \end{pmatrix}$ which expresses the relation between the molecular lattice and the grid of the Ag(111) surface. The calculated positions of the corresponding diffraction spots are indicated by the superimposed red circles in the right half of Fig. 1(c).

When comparing the monolayer structure of CuPc/Pb_1Ag_2 and CuPc/Ag(111), we find identical unit cell vectors length ($A = 13.99$ Å, $B = 13.77$ Å) and unit cell sizes ($F = 192.3$ Å^2) indicating a similar packing density of CuPc on both surfaces. The main differences between both superstructure lattices are the different angles between both unit cell vectors ($\Theta_{Pb1Ag2} = 86.2°$, $\Theta_{Ag(111)} = 96°$) and the different orientations of the superstructure unit cell with respect to the substrate lattice. These differences can be understood when considering the registry between the molecular superstructures and the substrate lattices. The CuPc monolayer structure on the surface alloy reveals a point-on-line registry with the lattice of the Pb_1Ag_2 alloy, but not with that of the Ag(111) surface. This is possible because of the 30° rotation of both surface lattices. On the other hand, on the bare Ag(111), CuPc does exhibit a point-on-line registry with the Ag(111) surface, but not with the (virtual) Pb_1Ag_2 lattice lines. Hence, in both cases, a point-on-line registry with the directly underlying metal layer is established. This indicates that the influence of the substrate on the structural properties of the molecular film is not vanishing for the modified Ag(111) surface layer. It causes different unit cells of the CuPc monolayer films and causes a point-on-line coincidence with the corresponding surface lattice.

A significantly different growth behavior is observed for PTCDA. We find clear indications that PTCDA forms long-range-ordered islands of its monolayer structure on the Pb_1Ag_2 surface alloy even for very low coverages. Changing the PTCDA coverage up to one monolayer does not lead to a change of the diffraction pattern, indicating an island growth of PTCDA with an unchanged structure. The corresponding diffraction pattern is shown in Fig. 1(d). The first-order diffraction spots of the surface alloy are still clearly visible, which indicates that the lateral order of the surface alloy is not affected by the adsorption of PTCDA. All diffraction spots

of the PTCDA monolayer structure can be unambiguously explained by one structural model with the superstructure matrix $\begin{pmatrix} 6 & 3 \\ 0 & 6 \end{pmatrix}$. The calculated positions of the diffraction spots of the corresponding structure are shown as red circles in the right half of Fig. 1(d). All diffraction spots of the Pb_1Ag_2 surface alloy can also be assigned to spots of the PTCDA monolayer. Consequently, the PTCDA monolayer structure is not only commensurate with the Ag(111) lattice, but also with the Pb-Ag surface alloy. This registry is the result of a rather strong influence of the Pb-Ag surface alloy on the structure formation of the PTCDA monolayer film leading to the existence of well-defined adsorption sites of PTCDA on Pb_1Ag_2.

The adsorption-site-specific interaction between PTCDA and the surface alloy is also the reason for the different size and shape of the PTCDA superstructure on the surface alloy and on the bare Ag(111) surface [1]. It is also responsible for the formation of two inequivalent PTCDA adsorption sites on the surface alloy which are occupied with a fixed ratio of 1:3 (see Sec. III B). At first glance, this is surprising since our LEED analysis yields a unit cell with only two PTCDA molecules. These contradicting observations can be resolved when considering that for highly symmetric molecular arrangements, diffraction spots with certain diffraction indices can be almost extinguished (see for instance [38]). Diffraction features with such low intensity can be easily missed in diffraction experiments. Therefore, we suspect that the true unit cell of the PTCDA monolayer structure on Pb_1Ag_2 is at least twice as large. Nevertheless, we can still unambiguously conclude that PTCDA adsorbs on distinct adsorption sites with respect to the Pb atoms as the PTCDA superstructure is commensurate with respect to the Pb-Ag surface alloy. This finding will become important when discussing the vertical adsorption geometry of PTCDA on the Pb_1Ag_2 surface alloy.

Note that recently a study on a similar system Bi_1Ag_2 surface alloy using local probe techniques was reported [24]. Cottin *et al.* reported the coexistence of two structural PTCDA phases on the surface, one long-range-ordered herringbone arrangement of PTCDA molecules and islands of disordered PTCDA molecules which are located close to domain boundaries and defects of the Bi-Ag surface alloy. However this growth behavior clearly differs from our results and we cannot adopt their structural model to gain insight into the adsorption sites of PTCDA/Pb_1Ag_2. Since there is no other reference system with similar lateral order, we refrain from proposing a real-space model for the local molecular adsorption geometry of PTCDA on the Pb_1Ag_2 surface alloy.

B. Core level spectroscopy

In this section we discuss our core level spectroscopy study performed for 1.0 ML CuPc and 0.8 ML PTCDA on the Pb_1Ag_2 surface alloy. All data were acquired in a grazing emission geometry of almost 90° and the secondary electron background was subtracted using the Shirley function [39].

The Pb 4f core level yields for both molecular films on the Pb_1Ag_2 surface alloy (blue and red curves) as well as for the bare surface alloy (black curve) are shown in Fig. 2. The spectrum of the bare surface alloy shows two emission lines that can be assigned to both spin-orbit split Pb 4f core levels. The asymmetric shape of these spectroscopic features is well

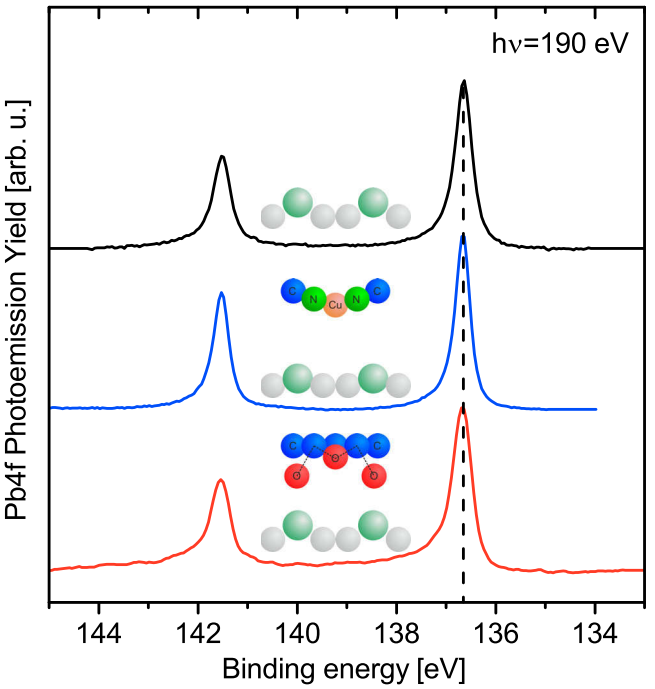

FIG. 2. Background-subtracted core level spectra for Pb 4f emission lines recorded for the pure Pb_1Ag_2 surface alloy (black curve), 1.0 ML CuPc/Pb_1Ag_2 (blue curve), and 0.8 ML PTCDA/Pb_1Ag_2 (red curve). The data were recorded in grazing emission geometry of almost 90°.

known for core level emission of metallic states and is caused by the many-body interaction in metals [40,41]. No shift can be observed in either of the emission lines upon adsorption of CuPc. This is in agreement with the absence of any vertical relaxation of the Pb atoms upon adsorption of CuPc discussed earlier [25]. Similarly, no shift of the Pb 4f lines was observed for the adsorption of PTCDA. However, a detailed line-shape analysis reveals a larger asymmetry of the Pb 4f emission lines upon adsorption of PTCDA. This change in line-shape could be the core level signature of the molecule-substrate hybridization, since this can lead to novel many-body effects and new screening possibilities of the created photohole. The latter are responsible for the core line shape in metals.

For the NIXSW analysis, the partial yield is obtained by the integrated intensity of the Pb 4$f_{7/2}$ emission line.

For CuPc, core level spectra were recorded for Cu 2p, N 1s, and C 1s. The core level spectra for N 1s and Cu 2p (not shown here) consist only of one single line. A possible difference between the two nitrogen species of CuPc could not be resolved.

For the C 1s spectra, both inequivalent carbon species of CuPc are clearly separated as illustrated in Fig. 3. The three spectroscopic features can be assigned to the C-C (1) and C-N carbon (2) species of the molecule as well as to the carbon satellite (blue line). In addition, a very broad energy loss tail (black line) can be observed at higher binding energies. This C 1s line shape is almost identical to the one of a metal phthalocyanine (MPc) multilayer film on noble-metal surfaces [42,43], but significantly different from the one of MPc monolayer films on Ag(111) [42,44]. This observation

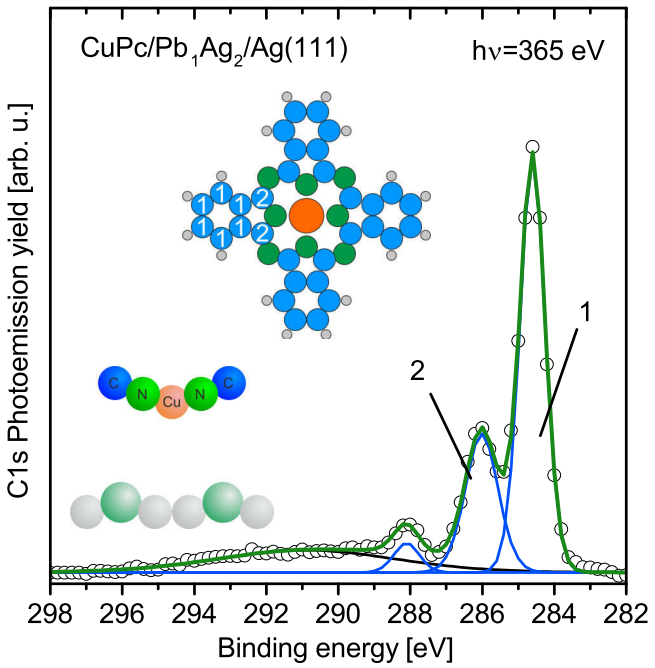

FIG. 3. Background-subtracted core level spectra for C 1*s* emission lines recorded for 1.0 ML CuPc/Pb_1Ag_2. The data were recorded in grazing emission geometry of almost 90°. Measured data points are shown as circles. The relevant core level components used in the fitting model are shown as blue solid lines and are labeled according to the molecule shown in the inset. The black solid line corresponds to a very broad energy loss tail and possibly some satellite structures.

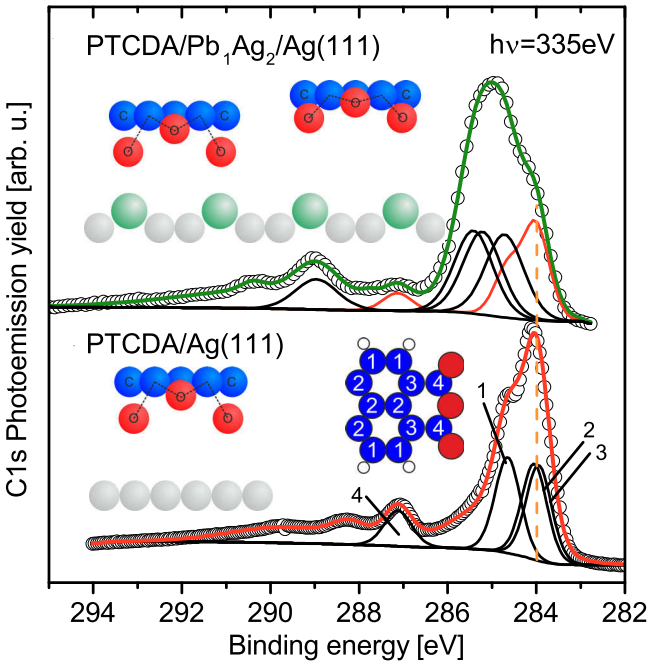

FIG. 4. Core level spectra for C 1*s* emission lines recorded for 0.8 ML PTCDA/Pb_1Ag_2 (upper part) and for a monolayer PTCDA/Ag(111) (lower part). The data were recorded in grazing emission geometry of almost 90°. Measured data points are shown as circles. For PTCDA/Ag(111) the fitting model was adapted from high-resolution core level data [45,46] and the relevant components are shown as solid black lines underneath the data. For PTCDA/Pb_1Ag_2, we had to consider two contributions from two inequivalent PTCDA molecules. In both cases, the broad satellite peak of the energy loss tail at high binding energies is omitted for clarity.

indicates a weak, van der Waals–like interaction between CuPc and the Pb_1Ag_2 surface alloy similar to the van der Waals–like interaction in molecular crystals.

The C 1*s* and O 1*s* core level signals for PTCDA on the Pb_1Ag_2 surface alloy are shown in the upper part of Figs. 4 and 5. As a reference, the lower part of both figures shows the corresponding core level signal for a monolayer PTCDA/Ag(111). First, we focus on the C 1*s* core level signal. The C 1*s* emission for PTCDA/Pb_1Ag_2 consists of an asymmetric main line that can be attributed to the different carbon species of the molecular backbone and a second emission feature at higher binding energies caused by carbon atoms directly connected to the oxygen end groups of PTCDA. When comparing this line shape to the one for PTCDA/Ag(111) several distinct differences can be observed: (i) For PTCDA/Pb_1Ag_2, the overall width of the main line is almost twice as large as for PTCDA/Ag(111). This already suggests a larger number of chemically different contributions to the C 1*s* core level emission. In addition, (ii) the asymmetry of the main line shows a shoulder at lower binding energies for PTCDA/Pb_1Ag_2 while the shoulder is found at higher binding energies for PTCDA/Ag(111).

To describe the complex line shape of the PTCDA/Pb_1Ag_2 core level data, we propose a fitting model based on two (electronically and geometrically) inequivalent PTCDA molecules on the surface. The different components of this fitting model are included as solid lines underneath the experimental data in Fig. 4. In our model, one PTCDA species shows the identical line shape and binding energy position as found for PTCDA/Ag(111) (red solid line). This contribution perfectly describes the low binding energy shoulder of the C 1*s* main line. Consequently, the high binding energy side of the main line is caused by the emission of the second PTCDA species. The best fitting result is obtained by the model shown as black curves. The latter reflects the C 1*s* line shape of a PTCDA multilayer film on Ag(111) [45]. Based on our detailed analysis we can conclude that the PTCDA film on the Pb_1Ag_2 surface alloy consists of two inequivalent PTCDA molecules occurring in a ratio of 1:3—one with a weak chemical interaction with the metal surface (species $PTCDA_A$ at adsorption site A), similar to PTCDA on Ag(111), and one with a weak van der Waals–like interaction (species $PTCDA_B$ at adsorption site B), similar to PTCDA on inert-noble-metal surfaces [46].

It is important to note at this point that $PTCDA_A$ is not caused by PTCDA molecules adsorbed on Pb free silver terraces. Instead, both electronically inequivalent PTCDA molecules are due to two inequivalent adsorption sites occurring within the PTCDA monolayer structure. This statement is supported by the following experimental findings: (i) As discussed, the adsorption height of the $PTCDA_A$ species is significantly higher compared to PTCDA/Ag(111) [47]. (ii) The C 1*s* line shape for PTCDA/Pb_1Ag_2 does not change for coverages below one monolayer, in accordance with our LEED study. (iii) Moreover, our recent momentum

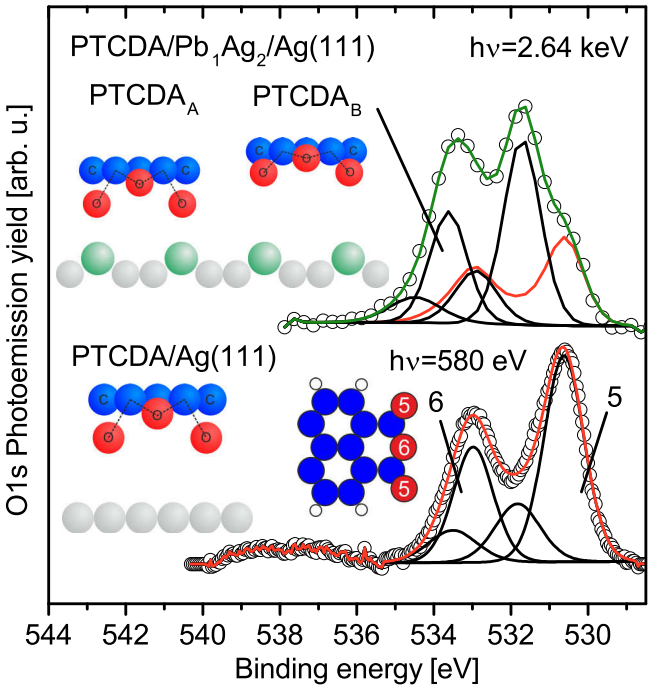

FIG. 5. Background-subtracted core level spectra for O 1*s* emission lines recorded for 0.8 ML PTCDA/Pb_1Ag_2 (upper part) recorded with hard x-ray radiation and for a monolayer PTCDA/Ag(111) recorded with soft x-ray radiation (lower part). The data were recorded in grazing emission geometry of almost 90°. Measured data points are shown as circles. For PTCDA/Ag(111) the fitting model was adapted from high-resolution core level data [45,46] and the relevant components are shown as solid black lines underneath the data. The broad satellite peak of the energy loss tail at high energies is omitted for clarity. For PTCDA/Pb_1Ag_2, we had to consider two contributions from two inequivalent PTCDA molecules.

microscopy study on the latter adsorbate system revealed a well-defined momentum space emission pattern with distinct maxima for the frontier molecular orbits of both inequivalent PTCDA species [25]. This indicates a similarly high degree of rotational order for both chemically different PTCDA species on sites A and B. Based on these findings we can unambiguously conclude that PTCDA/Pb_1Ag_2 grows in islands of its commensurate monolayer structure with a fixed ratio of PTCDA molecules on site A and site B of 1:3. Hence, PTCDA behaves differently on the Pb_1Ag_2 then on the corresponding Bi_1Ag_2 surface alloy on Ag(111) [24], a very similar system recently discussed by Cottin *et al.* These authors have found the formation of two coexisting PTCDA phases (i.e., in separated islands) each exhibiting one PTCDA species with different chemical interactions with the surface.

To obtain the partial yield curve of both PTCDA species for the NIXSW analysis, we constrained the width and the energy position of all peaks. In addition, we constrained the relative intensities of all signals stemming from the same molecule. As a result, we neglect any vertical distortion of the carbon backbone of both PTCDA species, for the benefit of a significantly lower number of fitting parameters.

The O 1*s* core level signal of PTCDA/Pb_1Ag_2 is shown in the upper part of Fig. 5. It reveals the typical line shape known for PTCDA on noble-metal surfaces with an additional shoulder on the low binding energy side. The two main peaks of the O 1*s* spectrum are attributed to two chemically inequivalent oxygen species of the anhydride end group of PTCDA, namely the carboxylic (5) and the anhydride (6) oxygen species. The intensity of both peaks does not reflect the stoichiometric ratio of 2:1 due to a rather complex satellite structure [23,47,48]. Additionally, we also expect two contributions from two inequivalent PTCDA molecules as already discussed above for the C 1*s* core level spectrum. The shoulder on the lower binding energy side is modeled by the line shape of the O 1*s* spectrum for a PTCDA monolayer film on Ag(111) (red solid line). For comparison, the O 1*s* data of a monolayer film PTCDA/Ag(111) is shown in the lower part of Fig. 5. The high binding energy part of the O 1*s* emission is modeled by the line shape of a PTCDA multilayer film [45,46] (black curves). The best-fitting quality was obtained for the model shown in Fig. 5. The binding energy position of the carboxylic main line of $PTCDA_B$ (black solid lines) is almost identical to the one for a PTCDA monolayer film on the inert noble-metal surface Au(111) [45]. Therefore, the O 1*s* core level analysis indicates two electronically and structurally inequivalent PTCDA molecules, in analogy to our findings for the C 1*s* core level emission.

For the partial yield curve, we again constrain the width and the energy position of all peaks. In addition, we constrained the relative intensities of all main peaks to their corresponding satellite structure. In this way, we will be able to disentangle the contributions of all chemically different oxygen species of both inequivalent PTCDA molecules.

C. Vertical adsorption geometry

In the following, we will discuss the vertical adsorption geometry for CuPc and PTCDA on the Pb_1Ag_2 surface alloy. Typical partial photoemission yield curves of individual NIXSW scans are shown in Fig. 6 for all chemical species that could be distinguished in the core level analysis. The uncertainty of each point in the photoemission yield curves was estimated by a Monte Carlo error analysis implemented in CASAXPS [23,49], the software we use for fitting the core level spectra. They are usually smaller than 10% and are omitted in Fig. 6 for clarity. The experimental results of the NIXSW analysis, the coherent position P^H and coherent fraction F^H, are obtained by fitting the photoemission yield curves using the NIXSW analysis software TORRICELLI [49].

Note that in the analysis of the Pb 4*f* partial-yield curves, nondipolar correction parameters had to be included in the analysis scheme in order to obtain physically reasonable coherent fractions in the range between 0 (homogeneous vertical disorder of all emitters) and 1 (perfect vertical order of all emitters). At first glance, this is rather surprising since nondipolar effects in the photoemission process are generally small due to the geometry used in our experiment, almost normal emission of the electrons (90°) with respect to the incident x-ray beam [50]. However, due to the large angular acceptance of the Scienta R4000 EW electron spectrometer of 30° in our experimental geometry, the photoemission yield also contains photoemission contributions from smaller emission angles for which nondipolar effects are known to

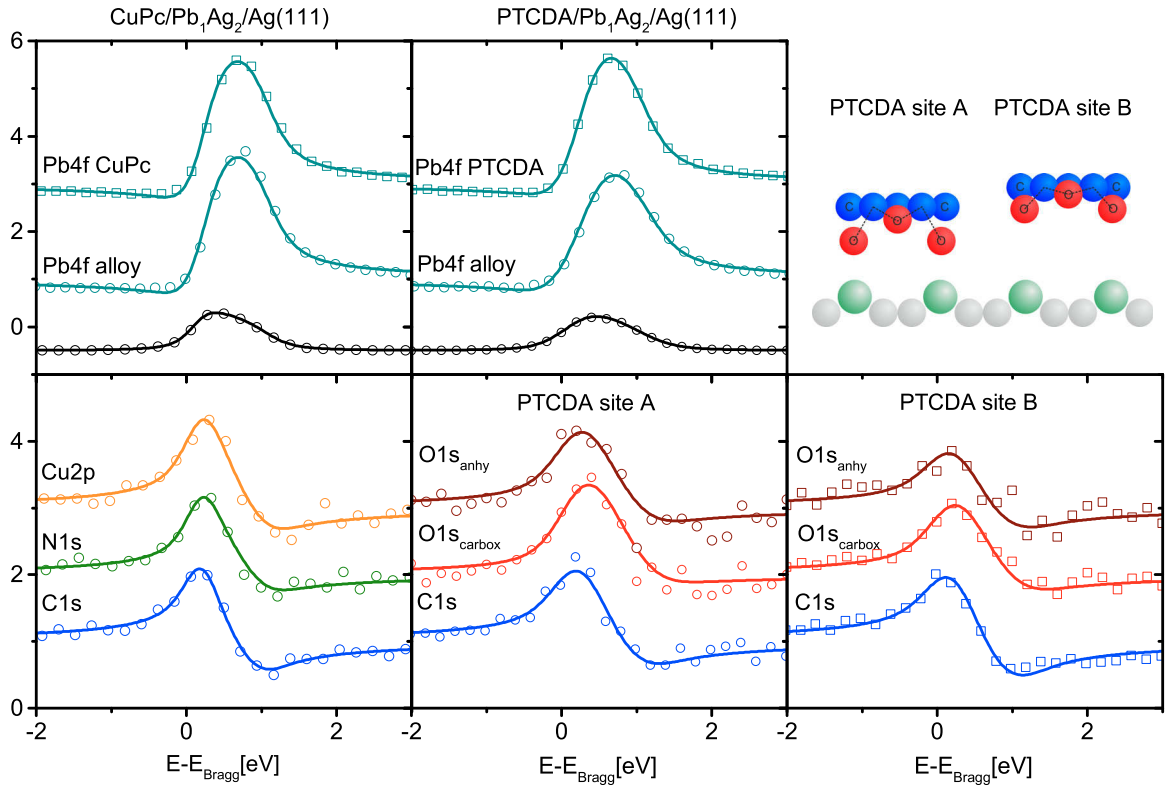

FIG. 6. Partial yield curves of single NIXSW scans for all distinguished species in the CuPc (left) and PTCDA (central and right panel) monolayer films on the Pb_1Ag_2 surface alloy, and reflectivity profiles of the substrate crystal (lowermost curves). Solid lines represent the best fit to the data obtained with the software TORRICELLI [49]. Note that, for each species, we have recorded several of these scans, usually between 3 and 5 scans, the results of which are presented in Fig. 7 for CuPc and in Fig. 9 for PTCDA.

influence the partial yield analysis in NIXSW experiments [50,51]. To estimate this effect, we separately analyzed the partial yield curves for different emission angles that were recorded in the angle-resolved detection mode of the R4000 EW photoemission spectrometer. While P^H stays constant within the experimental uncertainty for all emission angles, F^H increases continuously from values below 1.0 at an emission angle of 90° to 1.4 at ≈60°. In accordance with theoretical predictions, F^H is not significantly influenced by nondipolar effects at an emission angle of 90°; hence, the F^H value obtained for this emission angle reflects the correct coherent fraction for this atomic species. Comparing it with the result from the angle-integrated yield curve of the same NIXSW scan allows us to deduce nondipolar correction parameters for F^H for all Pb $4f$ scans ($S_R = 1.24$, $|S_I| = 1.12$, $\psi = 0$).

In the experiment, several NIXSW scans have been performed for the same atomic species on different spots on the sample. This will allow us to estimate the error in the NIXSW fitting parameters. The results of all individual scans for $CuPc/Pb_1Ag_2$ are plotted in the Argand diagram as data points in Fig. 7, for $PTCDA/Pb_1Ag_2$ in Fig. 9. In both Argand diagrams, arrows of the same color mark the average of the individual results for one species; the scattering of the data points around their mean values is a quantitative measure of their statistical error. The experimental uncertainty of the coherent fitting parameters and the adsorption height of each species are calculated by the standard deviation of the individual measurements. The averaged fitting parameters for P^H and F^H as well as the corresponding vertical adsorption position of each individual species are summarized in Table I for CuPc and in Table II for PTCDA. Except for Pb, all fitting results were obtained without considering possible nondipolar corrections. This could result in an overestimation of the coherent fraction which is typically in the same range as the experimental uncertainty, while the coherent position is barely affected. As reference, the adsorption heights of all atomic species of a CuPc [33] and PTCDA [47] monolayer film on the Ag(111) surface are also included in Table I and in Table II, respectively.

1. CuPc

First, we focus on the adsorption geometry of CuPc on the Pb_1Ag_2 surface alloy. The experimental data points of the NIXSW analysis for the Pb surface atoms prior to (cyan circles) and after (cyan squares) the adsorption of CuPc on the surface alloy are distributed around the same arithmetic means in the Argand diagram in Fig. 7. This clearly shows that the vertical relaxation of Pb is not altered by the adsorption of CuPc on the Pb_1Ag_2 surface alloy. Moreover, the coherent fraction F^H close to 1 is not modified by the adsorption of CuPc. This indicates the absence of any vertical disorder of the Pb atoms caused by the adsorption of CuPc; i.e., the geometric properties of the surface alloy are not altered by the interaction with CuPc.

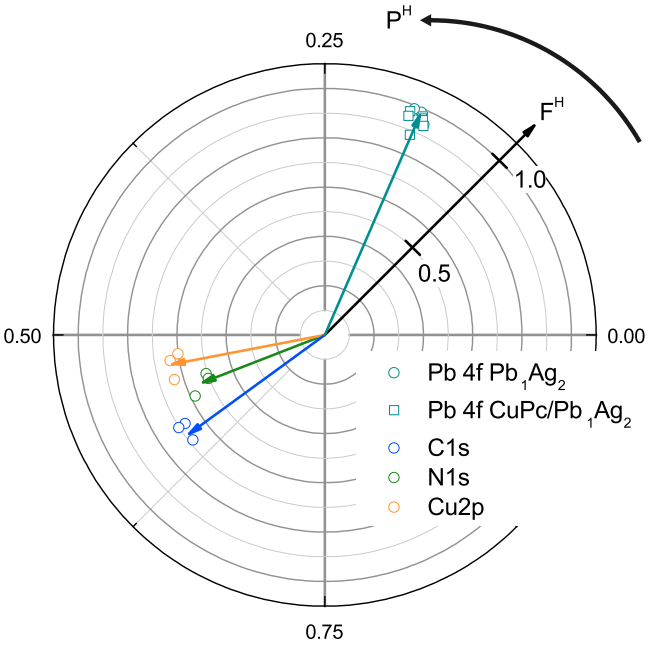

FIG. 7. Argand diagram illustrating the NIXSW fitting results for 1.0 ML CuPc/Pb_1Ag_2. The data points represent the fitting results of the individual NIXSW scans for each species; the mean values of all scans for each species are shown as vectors with identical color. The color code is identical to the one used for the yield curves in Fig. 6.

For further discussion, the vertical adsorption geometry of CuPc on the Pb_1Ag_2 alloy is shown in a true scale model in Fig. 8(a). As reference, a similar adsorption model of CuPc/Ag(111) is shown in Fig. 8(b). In both cases, the CuPc molecule and the metallic surface layer are drawn in a schematic side view. The dashed circles denote the nonbonding contact distance [52] which allows us to estimate the interaction strength across the interface.

On the surface alloy, CuPc adsorbs in a flat adsorption configuration similar to its adsorption on other noble-metal surfaces [33,53,54] with an average adsorption height of 3.7 Å. This vertical position of CuPc is significantly larger than its adsorption height of 3.08 Å on Ag(111). The different adsorption heights of CuPc for both systems is most likely caused by the larger size and the vertical relaxation of the Pb alloy atoms. As illustrated in the model in Fig. 8(a), CuPc is found at a vertical position that is only slightly smaller than the sum of the van der Waals radii of the corresponding atomic species of CuPc and the Pb atoms of the surface alloy, but clearly larger than the sum of the van der Waals radii of the CuPc species and the Ag surface atoms.

To quantify these findings, we normalize the adsorption heights to the sum of the van der Waals radii of the corresponding atomic species. These values $\Delta D^H_{\mathrm{CuPc-Pb/Ag}}$ are listed in Table I for CuPc on both the surface alloy and the pristine Ag(111) surface. The normalized distances $\Delta D^H_{\mathrm{CuPc-Ag}}$ between all species of CuPc and the Ag surface atoms are clearly larger than 1 indicating a vanishing overlap of electron density. In contrast, for the Pb-alloy surface we find an overlap between CuPc and Pb atoms similar to that for CuPc and Ag on the bare Ag(111) surface. Therefore, Pb atoms push the CuPc molecules away from the Ag surface atoms and prevent a (weak chemical) interaction between CuPc and the Ag surface atoms as observed for CuPc on Ag(111) [33].

2. PTCDA

We will now turn to the adsorption of PTCDA on the Pb_1Ag_2 surface alloy. The fitting results of the NIXSW analysis are summarized in the Argand diagram in Fig. 9. The fitting parameters of the Pb atoms before and after the adsorption of PTCDA (cyan circles and cyan squares, respectively) are clearly separated and the change of P^H points to a vertical relaxation of the Pb atoms of 0.06 ± 0.02 Å upon the adsorption of PTCDA. This value still underestimates the vertical displacement of the Pb atoms since the coverage of the PTCDA film investigated by NIXSW was below one monolayer ($\Theta_{\mathrm{PTCDA}} = 0.80$ ML). Therefore, the partial-yield curve still contains a 20% contribution of Pb atoms that are not covered by PTCDA molecules. To separate this contribution from the Pb atoms underneath the molecular film, we performed a vector component analysis [55].

In the Argand diagram, each XSW fitting result is represented by the vector $\mathbf{Z}(F^H, P^H) = F^H \cdot e^{2\pi P^H}$. When different adsorption heights occur for one species, this vector will be the sum of the Argand vectors representing the individual adsorption heights. Here, this is the case for the Pb atoms; i.e., their vector $\mathbf{Z}$ contains two contributions, one for Pb atoms underneath PTCDA molecules, $\mathbf{Z}_{\mathrm{Pb,PTCDA}}$, and one for Pb atoms without PTCDA molecules, $\mathbf{Z}_{\mathrm{Pb,alloy}}$. It can therefore

TABLE I. NIXSW fit results for 1.0 ML CuPc/Pb_1Ag_2. The numbers for P^H, F^H, and D^H_{alloy} are averaged values from the analysis of all individual NIXSW scans. Except for Pb, all fitting results were obtained without considering possible nondipolar corrections. The adsorption heights $D^H_{\mathrm{CuPc,ML}}$ of a monolayer film of CuPc/Ag(111) are included for comparison [33]. In addition, we calculated normalized adsorption heights of CuPc with respect to the Pb atoms $\Delta D^H_{\mathrm{CuPc-Pb}}$ and with respect to the Ag atoms $\Delta D^H_{\mathrm{CuPc-Ag}}$ of the Pb_1Ag_2 alloy. These distances are normalized to the sum of the corresponding van der Waals radii $r_C = 1.77$ Å, $r_N = 1.55$ Å, $r_{Cu} = 1.40$ Å, $r_{Ag} = 1.72$ Å, and $r_{Pb} = 2.02$ Å [52]. Similar normalized adsorption heights are calculated for a monolayer CuPc/Ag(111).

	P^H	F^H	D^H_{alloy} (Å)	$\Delta D^H_{\mathrm{CuPc-Pb}}$ (%)	$\Delta D^H_{\mathrm{CuPc-Ag}}$ (%)	$D^H_{\mathrm{CuPc,ML}}$ (Å)	$\Delta D^H_{\mathrm{CuPc,ML-Ag}}$ (%)
$Pb4f_{\mathrm{alloy}}$	0.187 ± 0.005	0.98 ± 0.03	0.44 ± 0.01				
$Pb4f_{\mathrm{CuPc}}$	0.187 ± 0.005	0.95 ± 0.04	0.44 ± 0.01				
$C1s_{\mathrm{CuPc}}$	0.60 ± 0.01	0.68 ± 0.02	3.77 ± 0.02	88	108	3.08 ± 0.02	88
$N1s_{\mathrm{CuPc}}$	0.56 ± 0.01	0.53 ± 0.05	3.68 ± 0.02	91	112	3.07 ± 0.04	94
$Cu2p_{\mathrm{CuPc}}$	0.53 ± 0.010	0.63 ± 0.04	3.62 ± 0.02	93	116	3.02 ± 0.04	97

TABLE II. NIXSW fit results for 0.8 ML PTCDA/Pb_1Ag_2. The numbers for P^H, F^H, and D^H_{alloy} are averaged values from the analysis of all individual NIXSW scans. Except for Pb, all fitting results were obtained without considering possible nondipolar corrections. The adsorption heights $D^H_{PTCDA,ML}$ of a monolayer film of PTCDA/Ag(111) are included for comparison [47]. In addition, we calculated normalized adsorption heights of all chemical species of both PTCDA molecules with respect to the Pb atoms $\Delta D^H_{PTCDA-Pb}$ and to the Ag atoms $\Delta D^H_{PTCDA-Ag}$ of the Pb_1Ag_2 alloy. These distances are normalized to the sum of the corresponding van der Waals radii $r_C = 1.77$ Å, $r_O = 1.52$ Å, $r_{Ag} = 1.72$ Å, and $r_{Pb} = 2.02$ Å [52]. Similar normalized adsorption heights are calculated for a monolayer PTCDA/Ag(111).

	P^H	F^H	D^H_{alloy} (Å)	$\Delta D^H_{PTCDA-Pb}$ (%)	$\Delta D^H_{PTCDA-Ag}$ (%)	$D^H_{PTCDA,ML}$ (Å)	$\Delta D^H_{PTCDA,ML}$ (%)
$Pb4f_{alloy}$	0.174 ± 0.008	0.92 ± 0.03	0.41 ± 0.02				
$Pb4f_{PTCDA}$	0.200 ± 0.005	0.94 ± 0.04	0.47 ± 0.01				
$Pb4f_{PTCDA,corr}$	0.206 ± 0.005	0.95 ± 0.04	0.49 ± 0.01				
$C1s_{PTCDA,A}$	0.54 ± 0.02	0.60 ± 0.09	3.63 ± 0.04	82	105	2.86 ± 0.01	82
$C1s_{PTCDA,B}$	0.61 ± 0.02	0.72 ± 0.12	3.80 ± 0.04	88	109	2.86 ± 0.01	82
$O1s_{carbox,A}$	0.41 ± 0.01	0.44 ± 0.10	3.33 ± 0.02	80	103	2.66 ± 0.02	82
$O1s_{carbox,B}$	0.53 ± 0.01	0.58 ± 0.04	3.61 ± 0.02	88	112	2.66 ± 0.02	82
$O1s_{anhy,A}$	0.49 ± 0.04	0.52 ± 0.05	3.52 ± 0.09	86	109	2.98 ± 0.08	92
$O1s_{anhy,B}$	0.59 ± 0.02	0.62 ± 0.03	3.74 ± 0.05	92	115	2.98 ± 0.08	92

be written as

$$\mathbf{Z} = a \cdot \mathbf{Z}_{Pb,PTCDA} + (1 - a) \cdot \mathbf{Z}_{Pb,alloy}, \quad (2)$$

where a is the fraction of the total yield arising from Pb atoms covered by PTCDA; i.e., a corresponds to the coverage of the molecular film.

Using this vector component analysis allows us to correct the vertical relaxation of the Pb atoms underneath PTCDA molecules to 0.08 ± 0.02 Å. Their coherent fraction, however, does not change due to the molecular adsorption. This indicates a similarly high vertical order of all Pb atoms before and after the adsorption of PTCDA and hence points to a homogeneous lifting of all Pb atoms of the surface alloy. At first glance, this finding is rather surprising as our core level analysis already revealed the existence of two inequivalent PTCDA species with different molecule substrate interaction strength. As will be discussed in detail below, we have strong evidence that the homogeneous vertical relaxation of all Pb atoms is caused by the formation of local (σ-like bonds) between the anhydride end groups of PTCDA and the Pb surface atoms. These types of bonds are formed between both PTCDA species and the Pb atoms of the surface alloy. Of course, small deviations in the vertical relaxation of the Pb atoms underneath the PTCDA molecules A and B cannot be excluded.

The NIXSW fitting results for all molecular species are shown in the left part of the Argand diagram in Fig. 9. For

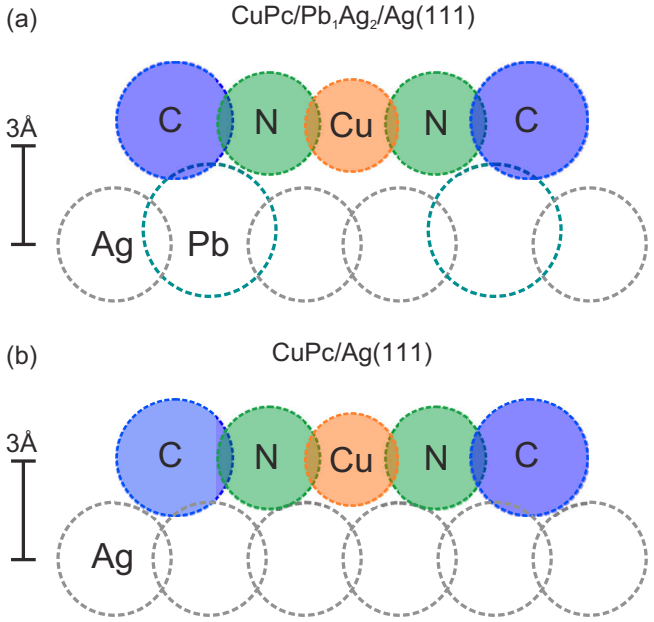

FIG. 8. Vertical true scale adsorption model for CuPc on the Pb_1Ag_2 alloy (a) and for CuPc/Ag(111) (b) [33]. The dashed circles denote the van der Waals radii of each atomic species [52].

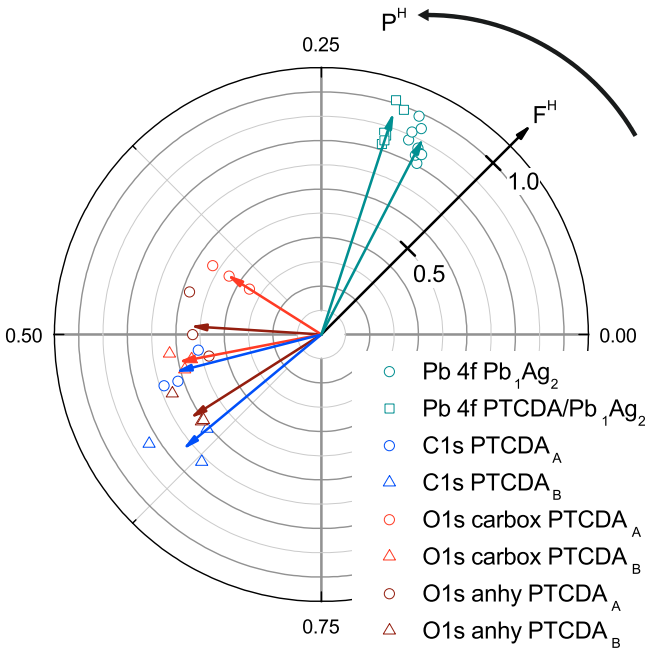

FIG. 9. Argand diagram illustrating the NIXSW fitting results for 0.8 ML PTCDA/Pb_1Ag_2. The data points represent the fitting results of the individual NIXSW scans for each species; the mean values of all scans for each species are shown as vectors with identical color. The color code is identical to the one used for the yield curves in Fig. 6.

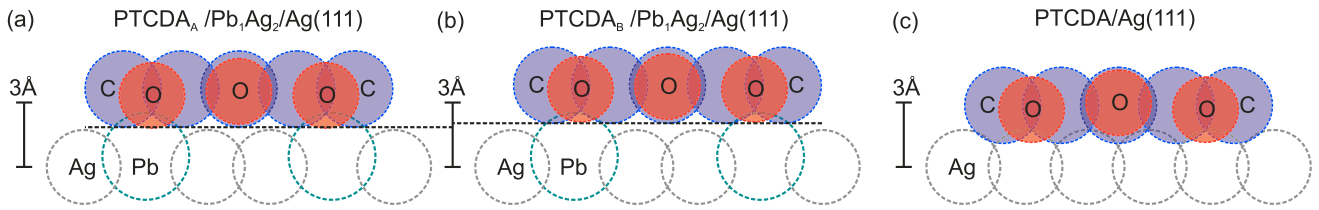

FIG. 10. Vertical true scale adsorption model for the structurally inequivalent PTCDA species PTCDA$_A$ and PTCDA$_B$ (b) on the Pb_1Ag_2 alloy as well as for PTCDA/Ag(111) (b) [47]. The dashed circles denote the van der Waals radii of each atomic species [52].

each species, the scattering of the data points around their arithmetic means is clearly larger compared to the data set recorded for CuPc. The resulting experimental uncertainties of the adsorption heights are $\leqslant \pm 0.05$ Å, except for the O1s$_{\text{anhy,A}}$ species where it is even ± 0.09 Å.

This large uncertainty is mainly due to the significantly more complex core level fitting model used to extract the partial yield curves for PTCDA. For the C 1*s* spectra we only consider two contributions to separate the average signal from both PTCDA species, while for the O 1*s* spectra we had to consider four contributions: two contributions for two chemically different oxygen species for each PTCDA species. In all cases, the individual contributions to the core level data show a large overlap in energy which makes a perfect separation of the corresponding signals rather challenging. However, the obtained adsorption height difference for equal chemical species of both inequivalent PTCDA molecules is still above the experimental uncertainties. This allows a clear separation of the vertical adsorption configurations of both geometrically inequivalent PTCDA molecules which are shown in a vertical true scale model in Figs. 10(a) and 10(b). Both molecules are drawn in a side view along their long molecular axis. For comparison, we have included a similar vertical true scale model for a monolayer film of PTCDA/Ag(111) [47] in Fig. 10(c). In analogy to the discussion for CuPc/Pb_1Ag_2, the dashed circles denote the van der Waals radii of the each element.

We now discuss the experimental observations for the two PTCDA species. Upon adsorption on the Pb_1Ag_2 surface alloy, both PTCDA species become distorted with respect to their planar geometry in the gas phase. Both oxygen species, the carboxylic and anhydride oxygen, are located below the carbon backbone leading to a M-like distortion of the molecules. The down-bending of all oxygen species of both types of PTCDA molecules and the homogeneous vertical displacement of all Pb atoms clearly indicate the formation of local O-Pb bonds between all oxygen atoms of both PTCDA molecules and the Pb surface atoms.

An M-like distortion of PTCDA was already reported for more reactive low-index noble-metal surfaces [5,56] but not for PTCDA molecules in homomolecular structures on Ag(111) [47]. On the latter surface, only the carboxylic oxygen atoms are located below the molecular plane while the anhydride oxygen atoms are located above. This leads to a saddle-like distortion of PTCDA. The transition from a saddle-like distortion on Ag(111) to an M-like distortion of PTCDA on Pb_1Ag_2 underlines the dominant role of σ-like O-Pb bonds for the interaction between both PTCDA species and the Pb_1Ag_2 surface alloy.

We will now focus on the adsorption height of the π-conjugated part of PTCDA, i.e., the carbon backbone, which allows us to deduce information about the formation of delocalized (chemical) bonds between the molecules and the surface alloy.

The carbon backbone of PTCDA$_A$ is located at an adsorption height of 3.63 Å, the one of PTCDA$_B$ at 3.80 Å. Both vertical positions are significantly larger than the adsorption height of PTCDA/Ag(111) [47]. In analogy to CuPc/Pb_1Ag_2, the larger adsorption height of both PTCDA species on the surface alloy compared to Ag(111) is caused by the larger atomic size of the Pb atoms, which pushes the PTCDA backbone away from the silver surface atoms. As illustrated in Figs. 10(a) and 10(b), this leads to a PTCDA-Ag bonding distance that is larger than the sum of the van der Waals radii of the involved species. As a result, the interaction between the aromatic part of PTCDA and the Ag surface atoms is completely suppressed. Quantitatively, this is also reflected in the normalized adsorption height $\Delta D^H_{\text{PTCDA-Ag}}$ shown in Table II. The calculated values are larger than 1 for both PTCDA species indicating a vanishing overlap between the molecular backbone and the Ag surface atoms.

In contrast, the PTCDA-Pb bonding distance is smaller than the corresponding nonbonding distance pointing to a delocalized interaction across the metal-organic interface. A quantitative analysis reveals that for PTCDA$_A$, the normalized adsorption distance $\Delta D^H_{\text{PTCDA-Pb}}$ is identical to the corresponding normalized distance for PTCDA/Ag(111) ($\Delta D^H_{\text{PTCDA,ML}}$). This suggests a weak chemical interaction between the π-conjugated part of PTCDA$_A$ and the Pb atoms similar to the interaction strength across the PTCDA/Ag(111) interface. This conclusion is in perfect agreement with a charge transfer and the corresponding population of the LUMO of PTCDA observed recently by momentum microscopy [25]. Hence, the geometric and electronic signatures of the molecule-substrate interaction provide conclusive evidence for the at least partial chemical interaction and the formation of a delocalized chemical bond between the π-conjugated part of PTCDA$_A$ and the Pb atoms of the surface alloy.

The normalized bonding distance between PTCDA$_B$ and the Pb atoms is larger than for PTCDA$_A$ and about halfway between the corresponding normalized bonding distance for PTCDA/Ag(111) and PTCDA/Au(111). While this finding clearly suggests a weaker PTCDA$_B$-Pb interaction compared to PTCDA$_A$-Pb, it does not allow an unambiguous classification of the molecule-substrate interaction strength. However, the C 1*s* core level line shape of PTCDA$_B$ is almost identical to the one for PTCDA/Au(111). The latter is a model system for a weak nonchemical molecule-substrate interaction. In

accordance, we conclude that the $PTCDA_B$-Pb interaction is dominated by (dispersive) van der Waals forces.

In conclusion, our NIXSW analysis reveals two distinct vertical adsorption geometries for PTCDA on the Pb_1Ag_2 surface alloy with different strength of the delocalized molecule-substrate bond. While the molecule-substrate bonding distance of $PTCDA_A$ suggests a weak chemical interaction between the molecule and the Pb surface atoms, the one of $PTCDA_B$ only points to a weak van der Waals–like bonding to the surface. We suspect that these different vertical adsorption geometries are caused by different adsorption sites of PTCDA on the surface alloy. The strength of the push-back effect depends on the exact position of the molecular carbon body on the Pb atoms and therefore is likely responsible for a site-specific interaction between PTCDA and the surface alloy.

IV. DISCUSSION

Our investigation of the vertical adsorption geometry of CuPc and PTCDA on the Pb_1Ag_2 surface alloy provides insight into how surface alloying can be used to alter the interactions and consequently the molecular properties at metal-organic hybrid interfaces. While both molecules reveal a weak chemical interaction with Ag(111), we observe three different adsorption scenarios on Pb_1Ag_2 with different interaction strength: (i) The first is found for $CuPc/Pb_1Ag_2$: The molecular adsorption height points to a weak van der Waals-like molecule-substrate bonding and CuPc essentially floats above the charge density spill-out of the surface mainly created by the Pb atoms.

The second and third scenarios are found for $PTCDA/Pb_1Ag_2$: Here two different adsorption configurations occur within the same molecular film. (ii) The backbone of one PTCDA species ($PTCDA_B$) is located at the same adsorption height as CuPc which points to a similarly weak van der Waals interaction between the π-conjugated part of this PTCDA species and the Pb surface atoms. However, the vertical positions of all oxygen atoms of $PTCDA_B$ below the molecular plane are a clear sign of the formation of local σ-like O-Pb bonds between PTCDA and the surface alloy. (iii) In contrast, we observe a clear overlap between the backbone of the second PTCDA species ($PTCDA_A$) and the Pb atoms comparable to the PTCDA-Ag overlap for PTCDA/Ag(111). Therefore, we detect the formation of an (at least partial) chemical bond between $PTCDA_A$ and the surface alloy. In addition, we also find clear indications for local O-Pb bonds for this PTCDA species.

To understand these different adsorption scenarios, we have to consider the adsorption heights and the corresponding charge reorganization for the reference systems CuPc/Ag(111) and PTCDA/Ag(111). Both interfaces are model systems with a weak chemical molecule-substrate interaction [5,7,33,47].

To first order, the molecular adsorption heights on inert-noble-metal surfaces are determined by the sum of the van der Waals radii of the carbon atoms of the molecular backbone and the surface atoms. The van der Waals radius of the surface atoms is a good way to model the vertical extent of the charge density spill-out of the noble-metal surface. Of course, the vertical electron density above the metal surface can be modified by the interaction between the molecule and the surface, i.e., by the push-back effect, hybridization between molecular and metal states, and charge transfer across the interface [5,17]. All these effects can reduce the evanescent electron density of the surface leading to molecular adsorption heights smaller than the sum of the van der Waals radii of the molecule and the surface.

Ab initio calculations [17] were able to show that CuPc acts as charge donor on the Ag(111) surface and repels the evanescent electron density back into the surface by the push-back effect, despite a small charge transfer into its LUMO level. In contrast, PTCDA becomes a charge acceptor on the Ag(111) surface and takes up charge from the surface in order to populate its LUMO level. This alters the vertical charge density profile of the metal surface which allows PTCDA to approach closer to the Ag(111) surface than CuPc. This qualitative model is also fully consistent with the adsorption height of CuPc and PTCDA on Ag(111) determined by NIXSW [33,47].

For the Pb_1Ag_2 surface alloy, the charge density above the surface is mainly determined by the Pb atoms due to their larger atomic size and their higher vertical position compared to Ag atoms. Consequently, the Pb atoms push both CuPc and PTCDA away from the surface and are hence responsible for the vanishing interaction between both molecules and the Ag surface atoms. Furthermore, the different adsorption height of CuPc and both PTCDA species on the Pb_1Ag_2 can also be understood by the different charge donating and accepting character of CuPc and PTCDA.

In analogy to its behavior on the Ag(111) surface, CuPc aims to reduce the vertical charge density above the surface by the push-back effect. Assuming a similar strength of the charge-donating character of CuPc on Ag and on the Pb-Ag surface alloy, CuPc suppresses a comparable fraction of the surface charge density and can approach the outermost surface atoms in a similar way. This is consistent with the experimental findings as the normalized bonding distance between CuPc and Pb for $CuPc/Pb_1Ag_2$ is very similar to the normalized bonding distance between CuPc and Ag for CuPc/Ag(111). The missing charge transfer into the CuPc LUMO is the most striking difference between the adsorption of CuPc on Ag and the Pb_1Ag_2 surface alloy [25]. We attribute this finding to the different electron configuration in the valence bands of Pb and Ag. While on bare noble-metal surfaces such as Ag and Cu the molecular levels interact mainly with *sp* bands of the substrate, the valence band structure of a surface containing Pb atoms is dominated by *p*-derived bands. The different orbital character of the valence band must hence be responsible for the missing hybridization between CuPc and the Pb_1Ag_2 surface.

For the adsorption site B of $PTCDA_B$, the adsorption scenario is rather similar. Due to the missing hybridization between the molecular π orbitals and the surface bands, the molecular backbone floats also on the vertical surface charge density which is only modified by the push-back effect. In particular, the local O-Pb bonds are not strong enough to pull the PTCDA molecules closer to the surface. This is clearly different for the adsorption site A of $PTCDA_A$. For this adsorption site, we suspect that the PTCDA molecule can initially approach the surface slightly farther then for the adsorption site of $PTCDA_B$. This results in the formation of shorter local O-Pb which are strong enough to pull the carbon

backbone of $PTCDA_A$ closer to the surface. Without additional charge reorganization at the interface, the lower adsorption height of the $PTCDA_A$ backbone would strongly enhance the push-back effect between the molecule and the surface. In extreme cases, such a behavior could even lead to a suppression of the Pb atoms back into the surface [56]. However, due to the strong electron affinity of PTCDA, a fraction of the surface charge density underneath the molecular backbone can be redistributed into LUMO of PTCDA, thereby reducing the push-back effect between the molecule and the surface. This leads to a partial population of the LUMO of $PTCDA_A$ as observed by momentum microscopy [25].

In conclusion, the existence of three different adsorption configurations for CuPc and PTCDA on Pb_1Ag_2 surface alloy is the result of the existence of site-specific local bonds between the molecules and the surface alloy as well as of the different charge donating and accepting properties of CuPc and PTCDA on noble-metal surfaces.

V. SUMMARY

In this paper, we have studied the vertical adsorption geometry of the prototypical molecules CuPc and PTCDA on a long-range ordered Pb_1Ag_2 surface alloy by the NIXSW technique. Two main experimental results were obtained: (i) CuPc and PTCDA are found at a significantly larger adsorption height on the Pb_1Ag_2 surface alloy than on Ag(111). At their respective vertical positions, the overlap of the molecular electron density and the Ag surface atoms vanishes completely. This points to a complete quenching of the partial chemical interaction between the molecules and the Ag atoms as it is known for their adsorption on Ag(111) [5,33,47]. (ii) Instead both molecules show a complex bonding to the Pb atoms of the surface alloy with three different interaction strengths: The large adsorption height of CuPc above the Pb_1Ag_2 surface alloy suggests that the interaction across the interface is mainly driven by van der Waals forces. For $PTCDA/Pb_1Ag_2$, we observe an adsorption-site-specific interaction that leads to two different adsorption heights. One PTCDA species ($PTCDA_B$) is located at the same adsorption height as CuPc pointing to a similarly weak van der Waals interaction between the π-conjugated part of this PTCDA species and the Pb surface atoms. The lower adsorption height of the second PTCDA species suggests a PTCDA-Pb π-bonding strength comparable to PTCDA/Ag(111), i.e., a weak chemical interaction. In addition, the vertical distortion of both PTCDA species points to the formation of local (σ-like) bonds between the functional oxygen groups of PTCDA and the Pb surface atoms.

The different adsorption heights for CuPc and PTCDA on Pb_1Ag_2 are the result of local site-specific molecule-surface bonds mediated by functional molecular groups and the different charge donating and accepting character of both molecules. For CuPc, a molecule with charge-donating character and without functional groups, the adsorption height is mainly determined by the push-back effect leading to an adsorption height close to the noncontact distance. In contrast, the local O-Pb bonds of PTCDA are strong enough to pull the π-conjugated part of PTCDA close to the surface and the charge-accepting character of PTCDA is responsible for the charge transfer into the PTCDA LUMO thereby reducing the charge density above the surface.

Hence, our results do not only underline the important role of local σ-like bonds for the interaction strength at metal-organic hybrid interfaces. They also show a route to tune and tailor the geometric and electronic properties of molecular films by controlling local, σ-like bonds using modified metal surfaces, i.e., by surface alloying.

ACKNOWLEDGMENTS

The experimental work was funded by the SFB/TRR 173 Spin+X: spin in its collective environment (Project B05) from the DFG. B.S. thankfully acknowledges financial support from the Graduate School of Excellence MAINZ (Excellence Initiative DFG/GSC 266). The authors would like to thank Pardeep Thakur and Tien-Lin Lee for their technical support at the beamline I09 of Diamond Light Source.

[1] L. Kilian, A. Hauschild, R. Temirov, S. Soubatch, A. Schöll, A. Bendounan, F. Reinert, T.-L. Lee, F. S. Tautz, M. Sokolowski *et al.*, Phys. Rev. Lett. **100**, 136103 (2008).

[2] C. Stadler, S. Hansen, I. Kröger, C. Kumpf, and E. Umbach, Nat. Phys. **5**, 153 (2009).

[3] J. Fraxedas, S. Garcia-Gil, S. Monturet, N. Lorente, I. Fernandez-Torrente, K. J. Franke, J. I. Pascual, A. Vollmer, R.-P. Blum, N. Koch *et al.*, J. Phys. Chem. C **115**, 18640 (2011).

[4] C. Wagner, D. Kasemann, C. Golnik, R. Forker, M. Esslinger, K. Müllen, and T. Fritz, Phys. Rev. B **81**, 035423 (2010).

[5] M. Willenbockel, D. Lüftner, B. Stadtmüller, G. Koller, C. Kumpf, S. Soubatch, P. Puschnig, M. G. Ramsey, and F. S. Tautz, Phys. Chem. Chem. Phys. **17**, 1530 (2015).

[6] N. Haag, S. Steil, N. Großmann, R. Fetzer, M. Cinchetti, and M. Aeschlimann, Appl. Phys. Lett. **103**, 251603 (2013).

[7] J. M. Gottfried, Surf. Sci. Rep. **70**, 259 (2015).

[8] D. G. de Oteyza, A. El-Sayed, J. M. Garcia-Lastra, E. Goiri, T. N. Krauss, A. Turak, E. Barrena, H. Dosch, J. Zegenhagen, A. Rubio *et al.*, J. Chem. Phys. **133**, 214703 (2010).

[9] G. Heimel, S. Duhm, I. Salzmann, A. Gerlach, A. Strozecka, J. Niederhausen, C. Brüker, T. Hosokai, I. Fernandez-Torrente, G. Schulze *et al.*, Nat. Chem. **5**, 187 (2013).

[10] A. Droghetti, S. Steil, N. Großmann, N. Haag, H. Zhang, M. Willis, W. P. Gillin, A. J. Drew, M. Aeschlimann, S. Sanvito *et al.*, Phys. Rev. B **89**, 094412 (2014).

[11] S. Müller, S. Steil, A. Droghetti, N. Großmann, V. Meded, A. Magri, B. Schäfer, O. Fuhr, S. Sanvito, M. Ruben *et al.*, New J. Phys. **15**, 113054 (2013).

[12] E. M. Reinisch, T. Ules, P. Puschnig, S. Berkebile, M. Ostler, T. Seyller, M. G. Ramsey, and G. Koller, New J. Phys. **16**, 023011 (2014).

[13] F. Bussolotti, S. Kera, and N. Ueno, Phys. Rev. B **86**, 155120 (2012).
[14] A. Tamai, A. P. Seitsonen, R. Fasel, Z.-X. Shen, J. Osterwalder, and T. Greber, Phys. Rev. B **72**, 085421 (2005).
[15] C. Zwick, A. Baby, M. Gruenewald, E. Verwüster, O. T. Hofmann, R. Forker, G. Fratesi, G. P. Brivio, E. Zojer, and T. Fritz, ACS Nano **10**, 2365 (2016).
[16] M. Cinchetti, S. Neuschwander, A. Fischer, A. Ruffing, S. Mathias, J.-P. Wüstenberg, and M. Aeschlimann, Phys. Rev. Lett. **104**, 217602 (2010).
[17] B. Stadtmüller, D. Lüftner, M. Willenbockel, E. M. Reinisch, T. Sueyoshi, G. Koller, S. Soubatch, M. G. Ramsey, P. Puschnig, F. S. Tautz *et al.*, Nat. Commun. **5**, 3685 (2014).
[18] C. Bobisch, T. Wagner, A. Bannani, and R. Möller, J. Chem. Phys. **119**, 9804 (2003).
[19] D. de Oteyza, E. Barrena, H. Dosch, J. E. Ortega, and Y. Wakayama, Phys. Chem. Chem. Phys. **13**, 4220 (2011).
[20] A. El-Sayed, P. Borghetti, E. Goiri, C. Rogero, L. Floreano, G. Lovat, D. J. Mowbray, J. L. Cabellos, Y. Wakayama, A. Rubio *et al.*, ACS Nano **7**, 6914 (2013).
[21] B. Stadtmüller, S. Schröder, and C. Kumpf, J. Electron Spectrosc. Relat. Phenom. **204**, 80 (2015).
[22] E. Goiri, P. Borghetti, A. El-Sayed, J. E. Ortega, and D. G. de Oteyza, Adv. Mater. **28**, 1340 (2016).
[23] G. Mercurio, O. Bauer, M. Willenbockel, B. Fiedler, T. Sueyoshi, C. Weiss, R. Temirov, S. Soubatch, M. Sokolowski, and F. S. Tautz, Phys. Rev. B **87**, 121409 (2013).
[24] M. Cottin, J. Lobo-Checa, J. Schaffert, C. Bobisch, R. Möller, J. Ortega, and A. Walter, New J. Phys. **16**, 045002 (2014).
[25] B. Stadtmüller, J. Seidel, N. Haag, L. Grad, C. Tusche, G. van Straaten, M. Franke, J. Kirschner, C. Kumpf, M. Cinchetti, and M. Aeschlimann, Phys. Rev. Lett. **117**, 096805 (2016).
[26] D. Pacilé, C. R. Ast, M. Papagno, C. Da Silva, L. Moreschini, M. Falub, A. P. Seitsonen, and M. Grioni, Phys. Rev. B **73**, 245429 (2006).
[27] N. Atodiresei, J. Brede, P. Lazić, V. Caciuc, G. Hoffmann, R. Wiesendanger, and S. Blügel, Phys. Rev. Lett. **105**, 066601 (2010).
[28] T. Methfessel, S. Steil, N. Baadji, N. Großmann, K. Koffler, S. Sanvito, M. Aeschlimann, M. Cinchetti, and H. J. Elmers, Phys. Rev. B **84**, 224403 (2011).
[29] S. Steil, N. Großmann, M. Laux, A. Ruffing, D. Steil, M. Wiesenmayer, S. Mathias, O. L. A. Monti, M. Cinchetti, and M. Aeschlimann, Nat. Phys. **9**, 242 (2013).
[30] K. Raman, N. Atodiresei, and J. Moodera, Spin **04**, 1440014 (2014).
[31] I. Gierz, B. Stadtmüller, J. Vuorinen, M. Lindroos, F. Meier, J. H. Dil, K. Kern, and C. R. Ast, Phys. Rev. B **81**, 245430 (2010).
[32] C. R. Ast, J. Henk, A. Ernst, L. Moreschini, M. C. Falub, D. Pacilé, P. Bruno, K. Kern, and M. Grioni, Phys. Rev. Lett. **98**, 186807 (2007).
[33] I. Kröger, B. Stadtmüller, C. Stadler, J. Ziroff, M. Kochler, A. Stahl, F. Pollinger, T.-L. Lee, J. Zegenhagen, F. Reinert *et al.*, New J. Phys. **12**, 083038 (2010).
[34] D. Woodruff, Prog. Surf. Sci. **57**, 1 (1998).
[35] D. Woodruff, Rep. Prog. Phys. **68**, 743 (2005).
[36] J. Zegenhagen, Surf. Sci. Rep. **18**, 202 (1993).
[37] F. Sojka, M. Meissner, C. Zwick, R. Forker, and T. Fritz, Rev. Sci. Instrum. **84**, 015111 (2013).
[38] B. Stadtmüller, I. Kröger, F. Reinert, and C. Kumpf, Phys. Rev. B **83**, 085416 (2011).
[39] D. Shirley, Phys. Rev. B **5**, 4709 (1972).
[40] G. K. Wertheim and S. Hüfner, Phys. Rev. Lett. **35**, 53 (1975).
[41] J. W. Gadzuk and M. Šunjić, Phys. Rev. B **12**, 524 (1975).
[42] M. Häming, C. Scheuermann, A. Schöll, F. Reinert, and E. Umbach, J. Electron Spectrosc. Relat. Phenom. **174**, 59 (2009).
[43] M. Nardi, F. Detto, L. Aversa, R. Verucchi, G. Salviati, S. Iannotta, and M. Casarin, Phys. Chem. Chem. Phys. **15**, 12864 (2013).
[44] J. L. Cabellos, D. J. Mowbray, E. Goiri, A. El-Sayed, L. Floreano, D. G. de Oteyza, C. Rogero, J. E. Ortega, and A. Rubio, J, Phys. Chem. C **116**, 17991 (2012).
[45] A. Schöll, Y. Zou, M. Jung, T. Schmidt, R. Fink, and E. Umbach, J. Chem. Phys. **121**, 10260 (2004).
[46] Y. Zou, L. Kilian, A. Schöll, T. Schmidt, R. Fink, and E. Umbach, Surf. Sci. **600**, 1240 (2006).
[47] A. Hauschild, R. Temirov, S. Soubatch, O. Bauer, A. Schöll, B. C. C. Cowie, T.-L. Lee, F. S. Tautz, and M. Sokolowski, Phys. Rev. B **81**, 125432 (2010).
[48] P. Unwin, D. Onoufriou, and T. Jones, Surf. Sci. **547**, 45 (2003).
[49] G. Mercurio, Ph.D. thesis, RWTH Aachen, 2012.
[50] J. J. Lee, C. J. Fisher, D. P. Woodruff, M. G. Roper, R. G. Jones, and B. C. C. Cowie, Surf. Sci. **494**, 166 (2001).
[51] C. Stadler, S. Hansen, A. Schöll, T.-L. Lee, J. Zegenhagen, C. Kumpf, and E. Umbach, New J. Phys. **9**, 50 (2007).
[52] A. Bondi, J. Phys. Chem. **68**, 441 (1964).
[53] I. Kröger, B. Stadtmüller, C. Kleimann, P. Rajput, and C. Kumpf, Phys. Rev. B **83**, 195414 (2011).
[54] H. Karacuban, M. Lange, J. Schaffert, O. Weingart, T. Wagner, and R. Möller, Surf. Sci. **603**, L39 (2009).
[55] B. Stadtmüller, M. Grunewald, J. Peuker, R. Forker, T. Fritz, and C. Kumpf, J. Phys. Chem. C **118**, 28592 (2014).
[56] O. Bauer, G. Mercurio, M. Willenbockel, W. Reckien, C. Heinrich Schmitz, B. Fiedler, S. Soubatch, T. Bredow, F. S. Tautz, and M. Sokolowski, Phys. Rev. B **86**, 235431 (2012).